Pignalberi *et al. Earth, Planets and Space* (2016) 68:93
DOI 10.1186/s40623-016-0466-5

Earth, Planets and Space

FULL PAPER Open Access

Comparison between IRI and preliminary Swarm Langmuir probe measurements during the St. Patrick storm period

Alessio Pignalberi[1], Michael Pezzopane[2*], Roberta Tozzi[2], Paola De Michelis[2] and Igino Coco[3]

Abstract

Preliminary Swarm Langmuir probe measurements recorded during March 2015, a period of time including the St. Patrick storm, are considered. Specifically, six time periods are identified: two quiet periods before the onset of the storm, two periods including the main phase of the storm, and two periods during the recovery phase of the storm. Swarm electron density values are then compared with the corresponding output given by the International Reference Ionosphere (IRI) model, according to its three different options for modelling the topside ionosphere. Since the Swarm electron density measurements are still undergoing a thorough validation, a comparison with IRI in terms of absolute values would have not been appropriate. Hence, the similarity of trends embedded in the Swarm and IRI time series is investigated in terms of Pearson correlation coefficient. The analysis shows that the electron density representations made by Swarm and IRI are different for both quiet and disturbed periods, independently of the chosen topside model option. Main differences between trends modelled by IRI and those observed by Swarm emerge, especially at equatorial latitudes, and at northern high latitudes, during the main and recovery phases of the storm. Moreover, very low values of electron density, even lower than 2×10^4 cm^{-3}, were simultaneously recorded in the evening sector by Swarm satellites at equatorial latitudes during quiet periods, and at magnetic latitudes of about $\pm 60°$ during disturbed periods. The obtained results are an example of the capability of Swarm data to generate an additional valuable dataset to properly model the topside ionosphere.

Keywords: IRI model, Swarm data, Topside electron density, St. Patrick storm

Introduction

At the end of 2013, the European Space Agency (ESA) launched the three-satellite Swarm constellation. Among the three satellites, two [Alpha (A) and Charlie (C)] are orbiting the Earth side-by-side at the same altitude of about 460 km, while the third [Bravo (B)] is flying about 60 km above. They are all equipped with identical instruments consisting of high-resolution sensors for measurements of both geomagnetic and electric fields, as well as plasma density. Besides the new generation instruments, the revolution introduced by this mission is in its geometrical configuration. For instance, satellites A and C allow performing differential investigations taking advantage of the proximity of the two satellites, while satellite B, whose orbital plane gets farther from that of the other two satellites, will allow spanning a wider local time window with consequent implications, for instance, for the Space Weather community (Friis-Christensen et al. 2006).

Here, we are interested mainly in the measurements made by the electric field instrument (EFI) comprising two thermal ion imagers (TIIs) and two Langmuir probes (LPs). The former measures the three-dimensional ion distribution, the latter the spacecraft potential, plasma density, and electron temperature, both at 2 Hz rate. In particular, we will analyze preliminary measurements of electron density (N_e) recorded by the Swarm constellation during March 2015, a period of time including the so-called St. Patrick storm. This storm, which was

*Correspondence: michael.pezzopane@ingv.it
[2] Istituto Nazionale di Geofisica e Vulcanologia, Via di Vigna Murata 605, 00143 Rome, Italy
Full list of author information is available at the end of the article

classified as severe and for which the K_p index reached the maximum value of 8, is the most intense observed during solar cycle 24. At ground observatories the sudden storm commencement was observed at around 04:45 Universal Time (UT) of 17 March 2015 with the arrival at the Earth of a coronal mass ejection. Figure 1 shows the temporal trend (from 9 to 25 March 2015) of the south component of the interplanetary magnetic field (IMF) and of some geomagnetic indices (D_{st}, AE, and a_p) describing the global level of the Earth's magnetic disturbance. The maximum intensity of the storm was reached at around 23:00 UT of 17 March and was characterized by the minimum value of D_{st} index of −223 nT. Some details on the complex structure of this storm can be found in Kamide and Kusano (2015) and Cherniak et al. (2015).

The vertical electron density profile is the most representative feature of the ionospheric plasma, and its reconstruction is essential for studies concerning ionospheric physics and for space weather purposes. Ground-based ionosondes can measure only the bottomside of this profile, up to the height of the F2-layer peak, that is the absolute maximum of the ionospheric electron density. With regard to the topside, from the F2-peak height to higher altitudes, ground-based ionosondes can provide only an estimation, based on bottomside measurements (Reinisch and Huang 2001; Huang and Reinisch 2001). Measuring the topside ionosphere requires an ionosonde onboard a satellite sounding from above the F2-peak. Only few missions from the sixties to the eighties, such as Alouette-1 and Alouette-2, ISIS-1 and ISIS-2, and Intercosmos 19, have provided sets of topside ionospheric data, but with a limited spatial coverage; moreover, only a small percentage of the total soundings were processed into electron density profiles (Huang et al. 2002). This lack of experimental topside ionospheric data (Benson et al. 1998) limits significantly the efforts to study and model this ionospheric region as a function of altitude and geographical location as well as diurnal, seasonal, and solar activity variations. Hence, even though, early in 2014, the International Reference Ionosphere (IRI) model was officially recognized as the international standard for the specification of the ionosphere by the International Standardization Organization (ISO) (Bilitza and Reinisch 2015), its topside profile often does not represent properly the real features of the ionosphere. A thorough description of these shortcomings and the corresponding efforts done to improve the model were published by Bilitza et al. (2006) and briefly summarized later in the section devoted to the IRI topside options illustration.

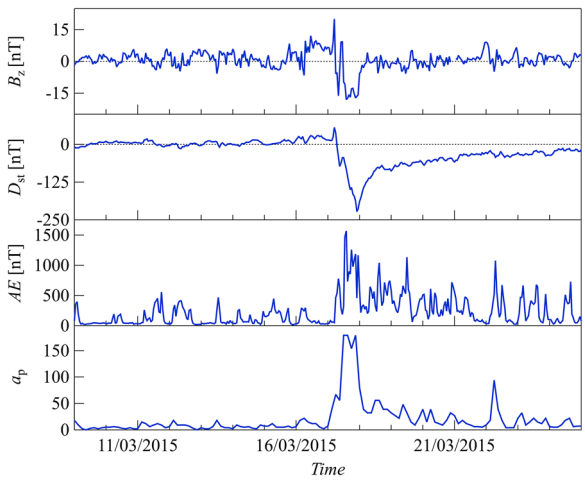

Fig. 1 B_z component of IMF and magnetic activity indices during the St. Patrick magnetic storm. From *top* to *bottom*: interplanetary magnetic field B_z component and D_{st}, AE, and 3-hourly a_p magnetic indices

Swarm satellites flight right in the topside ionosphere. In this paper, preliminary Swarm N_e measurements recorded during six time periods of March 2015 are considered and compared with the corresponding output given by the IRI model (Bilitza and Reinisch 2008; Bilitza et al. 2014). These time intervals are chosen to have two quiet periods before the onset of the storm, two periods including the main phase of the storm, and two periods during the recovery phase of the storm.

The Swarm N_e measurements, although preliminary and under validation, are considered nowadays reliable by the reference community. For example, Pedatella et al. (2015) did show a comparison between Swarm densities and those inferred from COSMIC radio occultation measurements and found a very good agreement: Overall, Swarm measurements seem to show a slight underestimate of the ionospheric electron density, varying between 8 and 15 % depending on latitude and local time.

Nevertheless, since the Swarm data validation is still ongoing, a comparison with IRI in terms of absolute values would have not been suitable. So, a correlation analysis was considered to evaluate the trends embedded in the Swarm and IRI time series. The corresponding results show that the representations made by Swarm and IRI are pretty different for both quiet and disturbed periods, independently of the chosen IRI topside option.

Methods

Swarm data

As already mentioned, data used consist of electron density measurements made onboard the three satellites of Swarm constellation during six selected time periods between 9 and 25 March 2015, a period of time including the so-called St. Patrick magnetic storm. During this

time window the only available data are those from the Preliminary Plasma Dataset prepared by the Swedish Institute for Space Science (IRF) at Uppsala (Knudsen et al. 2015). Specifically, only data with a quality flag value lower than 256 were considered (Knudsen et al. 2015).

The purpose of our investigation is to compare Swarm and IRI electron density representations for both disturbed and quiet magnetic conditions. For this reason, we chose two quiet periods before the onset of the St. Patrick storm which we refer to as pre-storm time intervals (P1 and P2), two periods characterized by a significant low value of the D_{st} index and including the main phase of the storm, which we refer to as main phase periods (M1 and M2), and two periods (R1 and R2) during the recovery phase of the storm. Detailed information on the bounds of the selected periods is summarized in Table 1, together with the range of variability and average values of D_{st} and *AE* indices in each period.

The pre-storm periods P1 and P2 were chosen according to simultaneously low values of both D_{st} and *AE* indices, in order to be quite confident that the magnetic activity was low at all latitudes. In fact, the well-known D_{st} index is able to represent the disturbance observed on the ground at low and mid-latitudes produced by the ring current, the partial ring current and by magnetopause and magnetotail currents during magnetic storms. Differently, *AE* index indicates the total intensity of the auroral electrojets and is used to represent the disturbance observed at high latitudes due to geomagnetic substorms. Consequently, when D_{st} is low, *AE* is not necessarily low as well. The main phase periods M1 and M2 correspond to the growth of the ring current till its maximum intensity and up to its initial decay, respectively. Values of D_{st} index during M2 still correspond to a significant perturbation of several tens of nanoTeslas in the horizontal component of the geomagnetic field, as observed at ground observatories. With regard to the recovery phase periods, R1 is selected midway, in terms of D_{st} index, between the main phase and quiet conditions, while during R2 quiet conditions are almost achieved.

In order to compare the 2 Hz Swarm N_e measurements with the N_e values provided by the IRI model at the same time and location, Swarm data are resampled, actually decimated, taking 1 every 9 measurements, which corresponds to a sampling of 4.5 s. This value descends by the fact that the IRI temporal step is expressed as tenths of hour, and at the same time has to be a multiple of 0.5 s, that is the Swarm sampling. The smallest value matching these two constraints is the decimal temporal increment of 0.00125 h which corresponds right to 4.5 s. The other temporal steps multiple of 0.5 s, and lower than 4.5 s, would give rise to circulating decimal temporal increments, which would result in an inaccurate analysis.

Data from each period shown in Table 1 are grouped according to magnetic local time (MLT) sectors and magnetic latitude bands. Partition into MLT is made to consider that, for each Swarm orbit, half measurements are taken in the morning sector (descending phase of satellite orbit) and half in the evening sector (ascending phase of satellite orbit). So, dividing data in this way we distinguish among the different dynamics characterizing morning and evening ionospheric sectors, especially at low and equatorial latitudes that are characterized by the fountain effect (Davies 1990; Kelley 2009). Since Swarm satellites move along near-polar orbits, MLTs are clustered around morning and evening sectors and partially spread over the entire 24 h MLT range at the poles. So, to consider disjoint set of measurements, the MLT ranges considered for the descending and ascending phases are 04–12 and 16–24 h. Within these time intervals, over 99 % of measurements taken between magnetic latitudes of 60°S and 60°N falls in the range 06–09 h for Swarm A and C and in the range 08–11 h for Swarm B, as concerns the morning sector, and in the range 18–21 h for Swarm

Table 1 Details on the time periods selected and on the corresponding level of magnetic activity expressed by means of D_{st} and *AE* geomagnetic indices

Period code	Day—start time [UT]	Day—end time [UT]	D_{st} [min, max] [nT]	$<D_{st}>$ [nT]	*AE* [min, max] [nT]	*<AE>* [nT]
P1	09—03 04:30:00	11—03 04:30:00	[−9, 15]	4	[22, 261]	57
P2	12—03 17:30:00	13—03 11:30:00	[−4, 12]	5	[−17, 259]	48
M1	17—03 00:00:00	17—03 23:59:59	[−223, 56]	−72	[37, 1570]	633
M2	18—03 00:00:00	18—03 23:59:59	[−189, −70]	−105	[200, 1043]	488
R1 (A)	19—03 00:00:00	20—03 11:57:33	[−88, −48]	−63	[61, 1134]	381
R1 (B)	19—03 00:00:00	20—03 03:42:33	[−88, −53]	−65	[61, 1134]	396
R1 (C)	19—03 00:00:00	20—03 23:59:59	[−88, −44]	−59	[61, 1134]	373
R2	24—03 00:00:00	25—03 23:59:59	[−36, 9]	−16	[28, 729]	165

Due to gaps in the 20 March Swarm A and B data, R1 time periods differ from satellite to satellite

A and C and in the range 20–23 h for Swarm B, concerning the evening sector. Differently, at latitudes higher than 60° the percentage of measurements taken in the morning and in the evening sectors decreases to around 60 %, being the orbits not really polar. Figure 2 shows the overall distribution of measurements in MLT without distinguishing between high and low/mid-latitudes.

The reason for the splitting into magnetic latitude bands is more or less the same as that related to the partition in MLT. In fact, most of processes occurring in the ionosphere have a marked magnetic latitudinal dependence (Davies 1990; Kelley 2009). So, we converted geographical coordinates into quasi-dipole coordinates (Emmert et al. 2010) and considered the following magnetic latitude bands: between −90°S and −60°S (SP, south pole), between −60°S and −30°S (SM, south mid), between −30°S and 30°N (EQ, equator), between 30°N and 60°N (NM, north mid), between 60°N and 90°N (NP, north pole). The limits of these bands have been chosen also on the base of the magnetic latitude distribution of Swarm N_e measurements. Two examples are shown in Fig. 3 for Swarm A, during the quiet period P1 for measurements recorded in the morning sector, and during the perturbed period M2 for measurements in the evening sector.

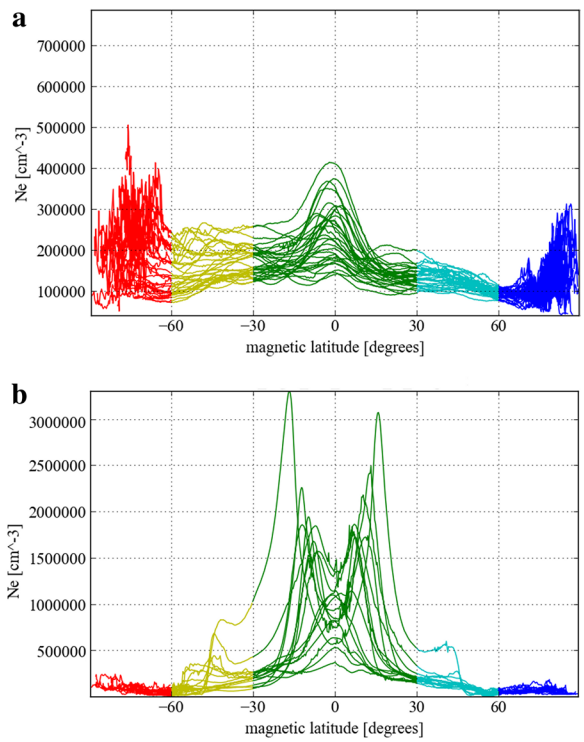

Fig. 3 Swarm A electron density during periods P1 and M2 in the morning and evening sector. Electron density as measured by Swarm A during **a** the pre-storm period P1 in the morning sector (04-12 MLT), and **b** during the main phase period M2 in the evening sector (16-24 MLT)

IRI model: topside electron density and storm options

Many studies have noted disagreements between the IRI topside modelling (hereafter called IRI-2001) and measurements (Bilitza 2001; Bilitza et al. 2006). IRI-2001 tends to overestimate the electron densities in the upper topside (from about 500 km above the F-peak upward) reaching a factor of about 3 at 1000 km above the ionospheric peak. In order to face this limitation two new options were introduced in IRI-2007 (Bilitza and Reinisch 2008). The first option (hereafter called IRI-2001corr) is a correction factor for the 2001 model, based on over 150,000 topside profiles from Alouette-1, Alouette-2, and ISIS-1, ISIS-2, and varying with altitude, modified dip latitude, and local time (Bilitza 2004). The application of this factor helped, for instance, in improving the discrepancies that were found by Jee et al. (2005), who compared IRI-2001 with TOPEX measurements.

The second option (hereafter called IRI-NeQuick) is the NeQuick topside model (Radicella and Leitinger 2001; Coisson et al. 2006). This model is based on a semi-Epstein layer function, governed by an empirical shape parameter k, whose analytical relationship was first calculated by using TEC data and ionosonde data recorded respectively at Florence and Rome, Italy (Radicella and Zhang 1995), and subsequently updated by using ISIS-2 topside profiles (Coisson et al. 2006). Comparisons with

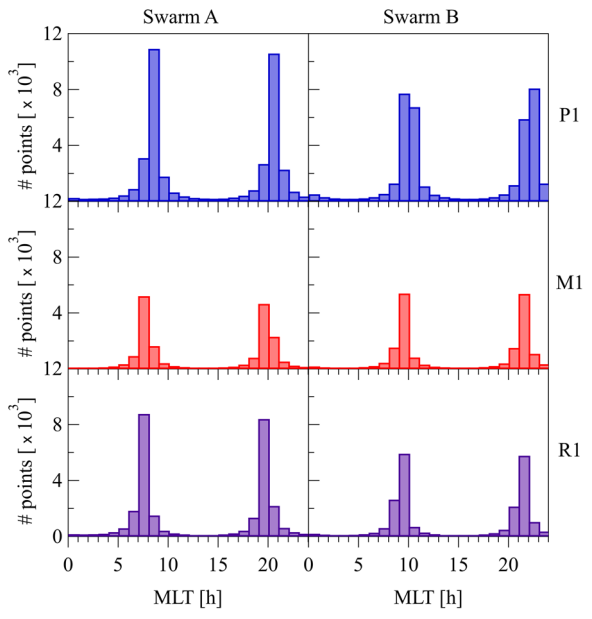

Fig. 2 Electron density value availability for Swarm A and B. Histograms of available electron density measurements as a function of MLT, for P1, M1, and R1, for Swarm A and B. Due to the geometry of Swarm constellation the MLT distribution of Swarm C is identical to that of Swarm A

TOPEX data have shown that IRI-NeQuick provides an improvement with respect to IRI-2001 predictions (Coisson et al. 2004).

Since the IRI-2001 version, also a storm option as a correction factor for disturbed conditions is included (Fuller-Rowell et al. 2000; Bilitza 2001; Araujo-Pradere et al. 2002). This option consists of an empirical ionospheric storm-time correction model that scales the quiet time F region critical frequency (*fo*F2) to account for storm-time changes in the ionosphere. IRI uses the 3-hourly a_p index for the description of magnetic storm effects, and the storm model option is driven by a new index based on the integral of the a_p index over the previous 33 h, weighted by a filter obtained by the method of singular value decomposition. The storm option gives reliable results at mid-latitudes during summer and equinox, but during winter and near the equator, the model does not improve significantly the IRI representation.

It is worth highlighting that the IRI storm model option was implemented mostly to represent the mid-latitude F2 peak density variations for disturbed conditions. Anyhow, the setting on of this option clearly influences the whole electron density profile over the entire terrestrial globe. With regard to this, Fig. 4 displays six global maps of the following percent relative difference

$$\left[\frac{(\mathrm{IRI}-\mathrm{NeQuick})_{\mathrm{StOFF}}-(\mathrm{IRI}-\mathrm{NeQuick})_{\mathrm{StON}}}{(\mathrm{IRI}-\mathrm{NeQuick})_{\mathrm{StOFF}}}\right]\times 100 \tag{1}$$

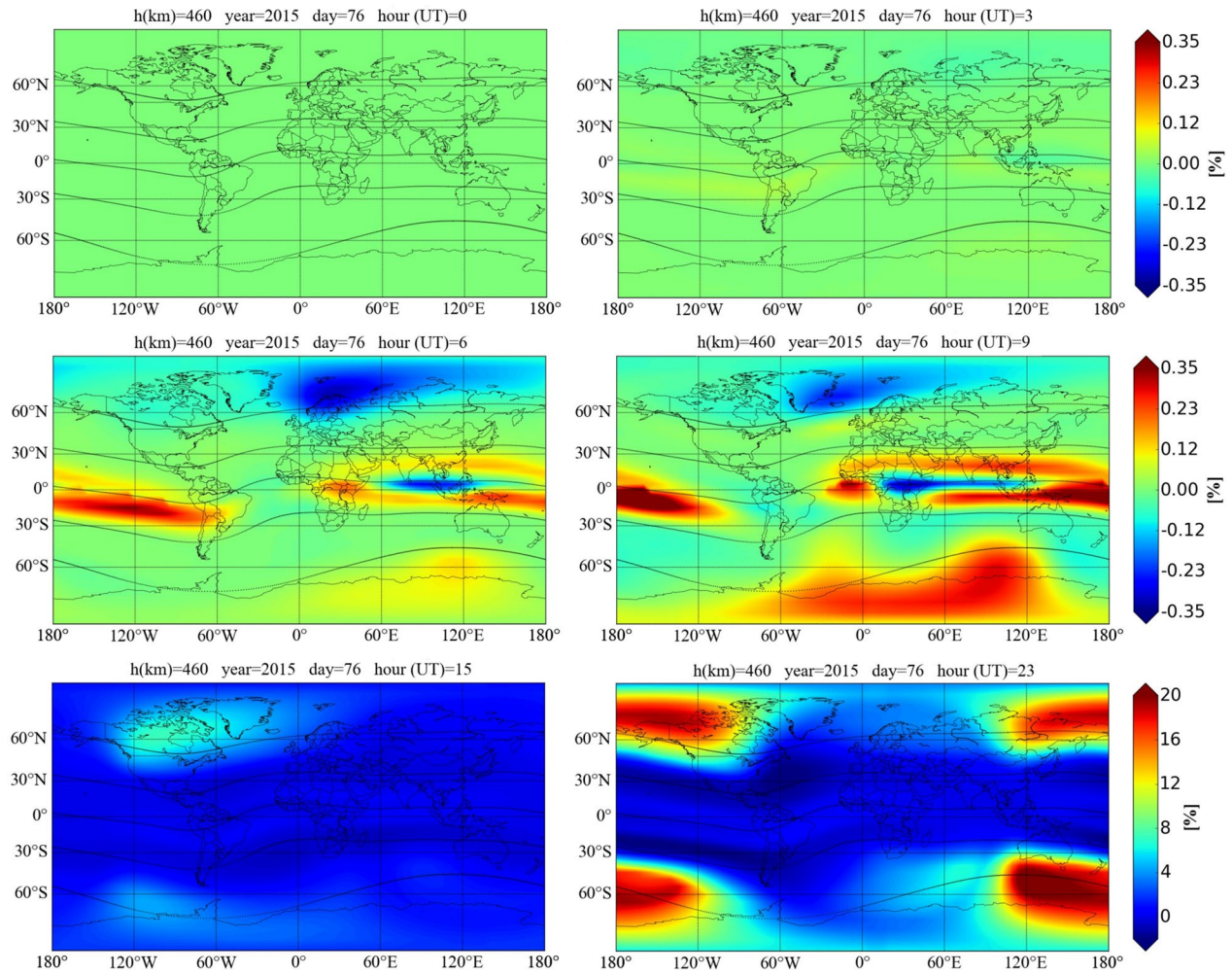

Fig. 4 Percent relative difference between IRI model StOFF and StON on 17 March 2015. Electron density percent relative difference according to Eq. (1) on 17 March 2015 at 00, 03, 06, 09, 15, and 23 UT, at 460 km of altitude. Coordinates are geographical. *Bold lines* represent the magnetic parallels at −60°, −30°, 0°, 30°, and 60°. Due to the large difference between N_e values for different times, it is not possible to use the same *color scale* for all *plots*

between the electron densities given by IRI-NeQuick with the storm option off (StOFF) and the electron densities given by IRI-NeQuick with the storm option on (StON), on 17 March 2015 at 00, 03, 06, 09, 15, and 23 UT, at 460 km of altitude, that is the orbital altitude of Swarm A and C. It is evident that at 00 UT, before the beginning of St. Patrick storm, the two representations are identical, with the corresponding percent difference equal to 0 % everywhere; on the contrary, when the storm is ongoing, differences between StON and StOFF appear and become more and more significant.

Analysis

In this work, the IRI model is used to estimate N_e at the same time and location (geographical latitude and longitude, altitude) of Swarm measurements falling in the six selected periods listed in Table 1. In detail, we used the URSI coefficients, according to the three topside options (IRI-2001, IRI-2001corr, NeQuick), and with the storm option on (StON).

Among all the plots that were obtained, only a few are shown as representative in Figs. 5, 6, 7, 8, 9, 10, 11, and 12. These figures compare, for morning (Figs. 5, 6, 7, 8) and evening (Figs. 9, 10, 11, 12) sectors, electron densities measured by Swarm A with the corresponding ones calculated by IRI-NeQuick(StON), and electron densities measured by Swarm B with the corresponding ones calculated by IRI-2001corr(StON), for periods P1, M1, M2, and R1. With regard to these figures, it is worth noting that showing Swarm A measurements only with the output given by the NeQuick option, and Swarm B measurements only with the output given by the IRI-2001corr option, does not mean that the other topside options were not considered to perform the comparison. This way to proceed was imposed only by the fact that it was clearly not possible to show for each time period listed

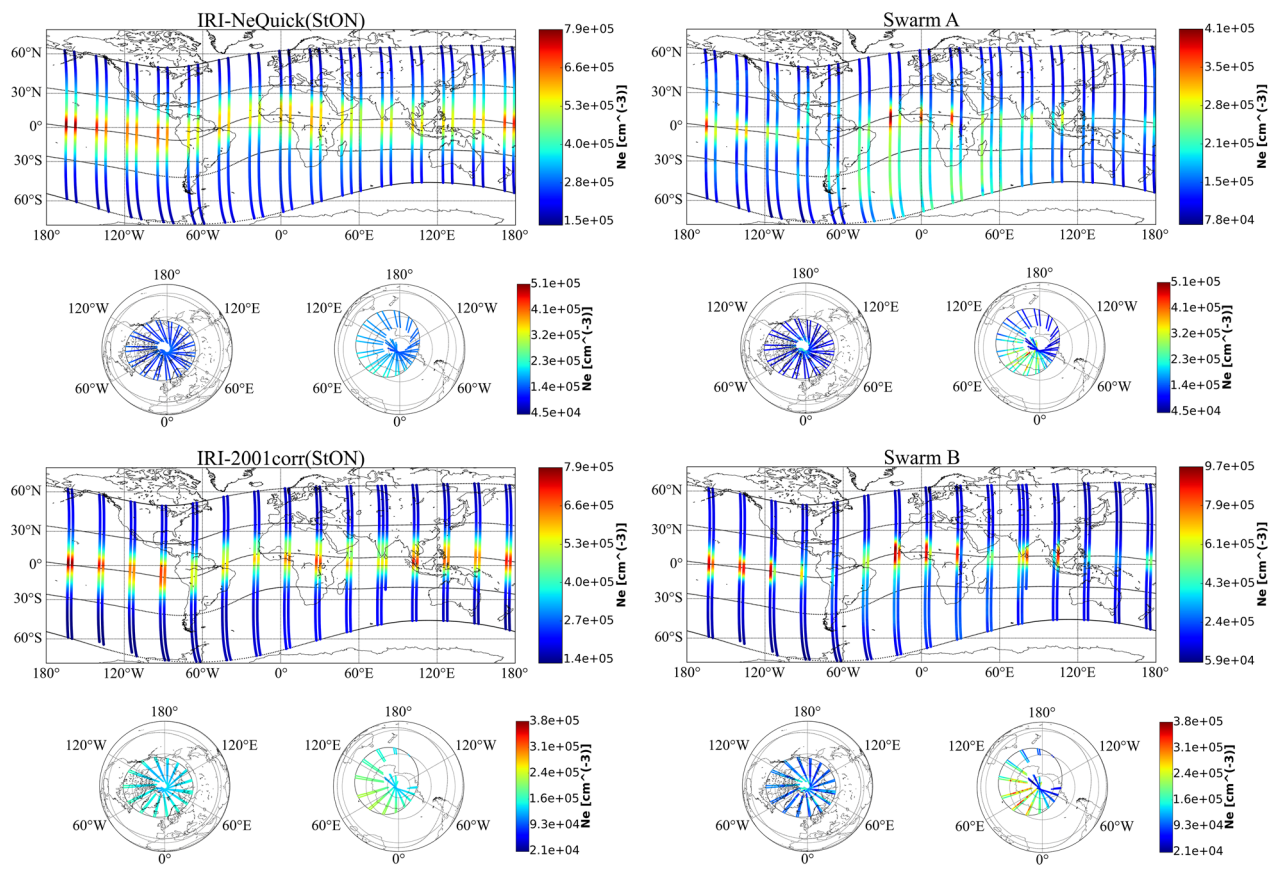

Fig. 5 Electron densities measured by Swarm satellites and IRI for period P1, for the morning sector. Electron densities measured by Swarm A (*top-right panels*) and Swarm B (*bottom-right panels*), and the corresponding ones calculated by IRI-NeQuick(StON) (*top-left panels*) and IRI-2001corr(StON) (*bottom-left panels*), for the period P1, for the morning sector. Magnetic latitude bands between −60° and 60° are plotted in a Gall stereographic projection, while the high-latitude bands are plotted in an orthographic projection (*on the left* the north pole, *on the right* the south pole). Coordinates are geographical, and *bold lines* in both Gall stereographic projections and polar orthographic projections represent magnetic parallels drawn with a 30° step. Due to the large difference between N_e values measured by Swarm A and B and those estimated by IRI, it is not possible to draw the values into the Gall stereographic projections with the same *color scale*

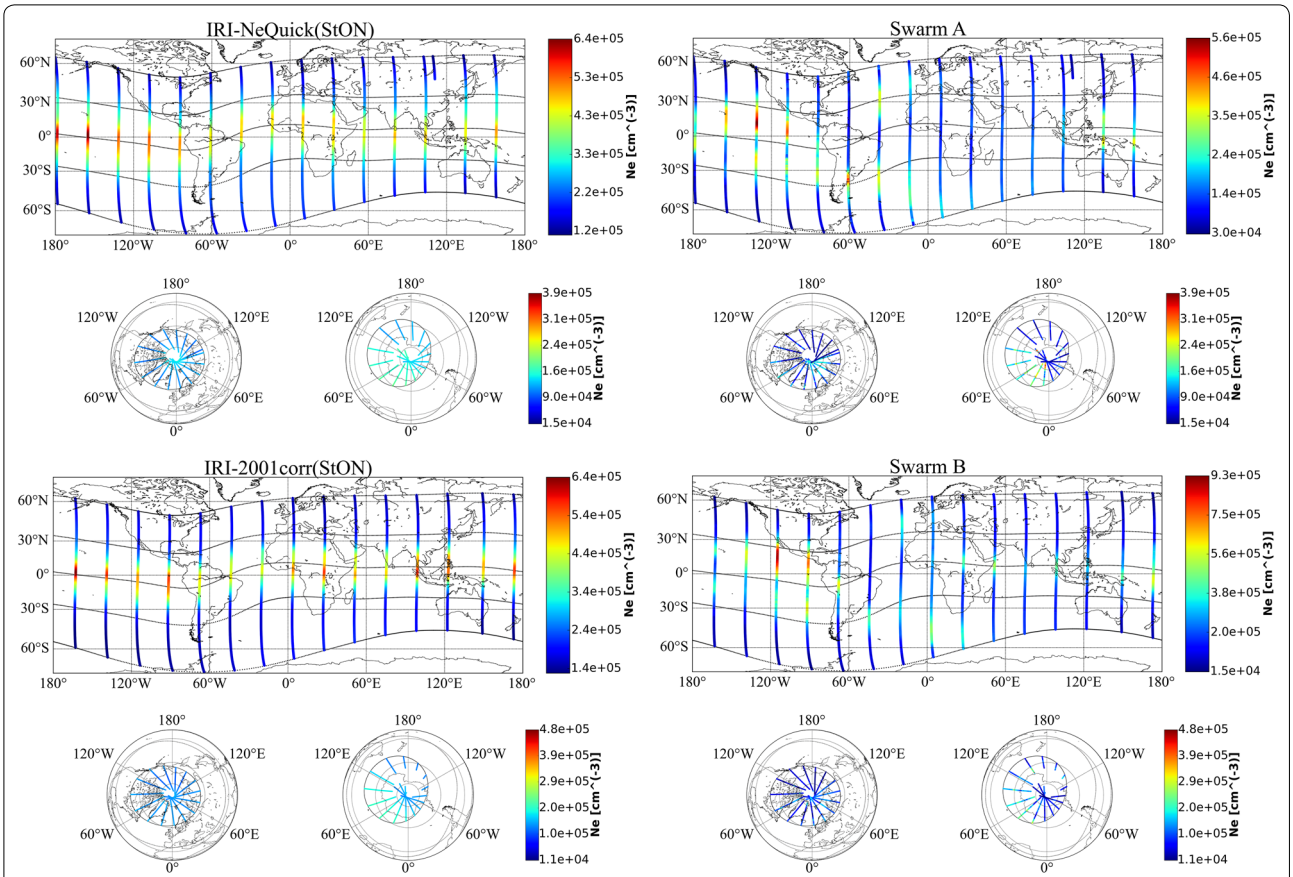

Fig. 6 Electron densities measured by Swarm satellites and IRI for period M1, for the morning sector. Same as Fig. 5, but for M1 morning sector

in Table 1 the corresponding output given by each of the three IRI topside options. Moreover, at Swarm altitudes, the three IRI topside options give a very similar ionospheric representation, and that's why we chose to represent different IRI topside options for Swarm A and B.

In order to assess quantitatively the behavior of the different IRI topside models, for each selected period, and for each model, the Pearson correlation coefficient between Swarm and IRI time series was calculated, according to the following formula

$$\rho_{X,Y} = \frac{\mathrm{cov}(X,Y)}{\sigma_X \sigma_Y} = \frac{E((X - E(X))(Y - E(Y)))}{\sigma_X \sigma_Y}, \qquad (2)$$

where cov() is the covariance between the variables X and Y, σ_X e σ_Y are the corresponding standard deviations, and $E()$ represents the expected value.

We chose this approach because the Swarm Langmuir probe data are still undergoing a thorough validation, and hence, a comparison in terms of absolute values would have not been appropriate. On the contrary, the value of the Pearson coefficient can give an idea about the similarity of trends embedded in the IRI and Swarm time series.

Figures 13 and 14 show the average of Pearson coefficients calculated for Swarm A and C, and Pearson coefficients calculated for Swarm B, by considering all the three IRI topside options (IRI-2001, IRI-2001corr, NeQuick), respectively, for morning and evening sectors, and for each magnetic latitude band. Correlations for Swarm A and C were averaged since obtained results are practically identical. Figure 15 displays instead the magnetic latitude dependence of Pearson coefficients shown in Figs. 13 and 14.

In the analysis we have done, we noted that sporadically Swarm data were characterized by very low values of electron density, even lower than 2×10^4 cm^{-3}. To assess the truthfulness of these values, we checked whether they were recorded simultaneously by Swarm A and C, and we found that these values were seen by both satellites. As expected, these unusually low values are not reproduced by the IRI model. As an example, Fig. 16 shows where Swarm A (the same is for Swarm C) recorded these values for periods P1, M2, and R1, for the evening sector. For the morning sector, these low values are practically absent.

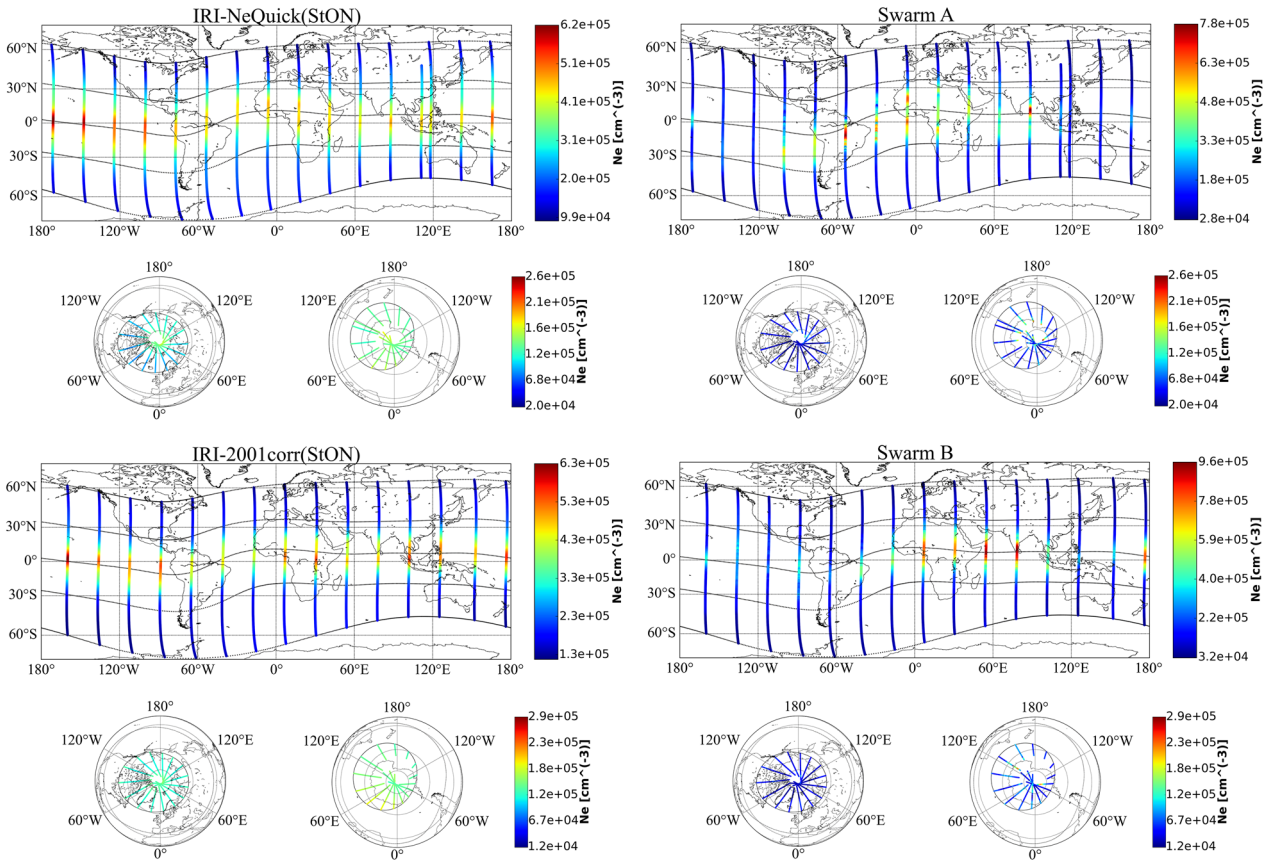

Fig. 7 Electron densities measured by Swarm satellites and IRI for period M2, for the morning sector. Same as Fig. 5, but for M2 morning sector

Results and discussion

Before getting to the hearth of the discussion of results, we want to draw the attention to the fact that in this section each time we talk generically about Swarm, we refer to all satellites (Swarm A, B, and C), and each time we talk about Swarm A, due to their proximity, we are implicitly talking also about Swarm C. Moreover, if we look carefully at Figs. 13, 14, and 15, we realize that: (a) the differences between the correlation coefficients of IRI-2001 and those of IRI-2001corr are minimal; (b) even though the correlation coefficients of IRI-NeQuick can be different from those of IRI-2001 and IRI-2001corr, the corresponding trend is, however, somewhat similar. So, henceforward, when we talk about IRI, we mean that the same is valid for all the corresponding three topside models.

Looking at Figs. 5, 6, 7, 8, 9, 10, 11, and 12, several interesting features measured by Swarm satellites, and differences between these and IRI, come out. Below, first are discussed the results of morning sectors of Figs. 5, 6, 7, and 8, and then the results of the corresponding evening sectors of Figs. 9, 10, 11, and 12.

Concerning the period P1 (the same is for period P2), for the morning sector (Fig. 5), the equatorial band shows for both IRI and Swarm the same usual pattern characterized by a maximum of electron density along the magnetic equator (e.g., Balan and Bailey 1995). Anyway, some differences about the electron density intensity appear: Swarm A measures N_e values lower than those calculated by IRI, while the contrary holds for Swarm B. This dissimilarity could be related to the local time shift characterizing the two satellites (see Fig. 2) but, more likely, is due to their different orbital altitudes, a fact that, when having accurate measurements, will turn out to be really useful to obtain new insights about the topside plasma scale height, which is so important to reliably model the topside profile. In Fig. 5, as reported also by several authors (Sagawa et al. 2005; Immel et al. 2006; Liu et al. 2010; Lühr et al. 2012; Xiong and Luhr 2014) a wave-3 longitudinal modulation is discernible, more evident for Swarm B than for Swarm A; IRI succeeds in catching this feature only modelling the same times and locations of Swarm B. Figure 5 shows also, for Swarm A, a general underestimation made by IRI in the southern part of Atlantic Ocean.

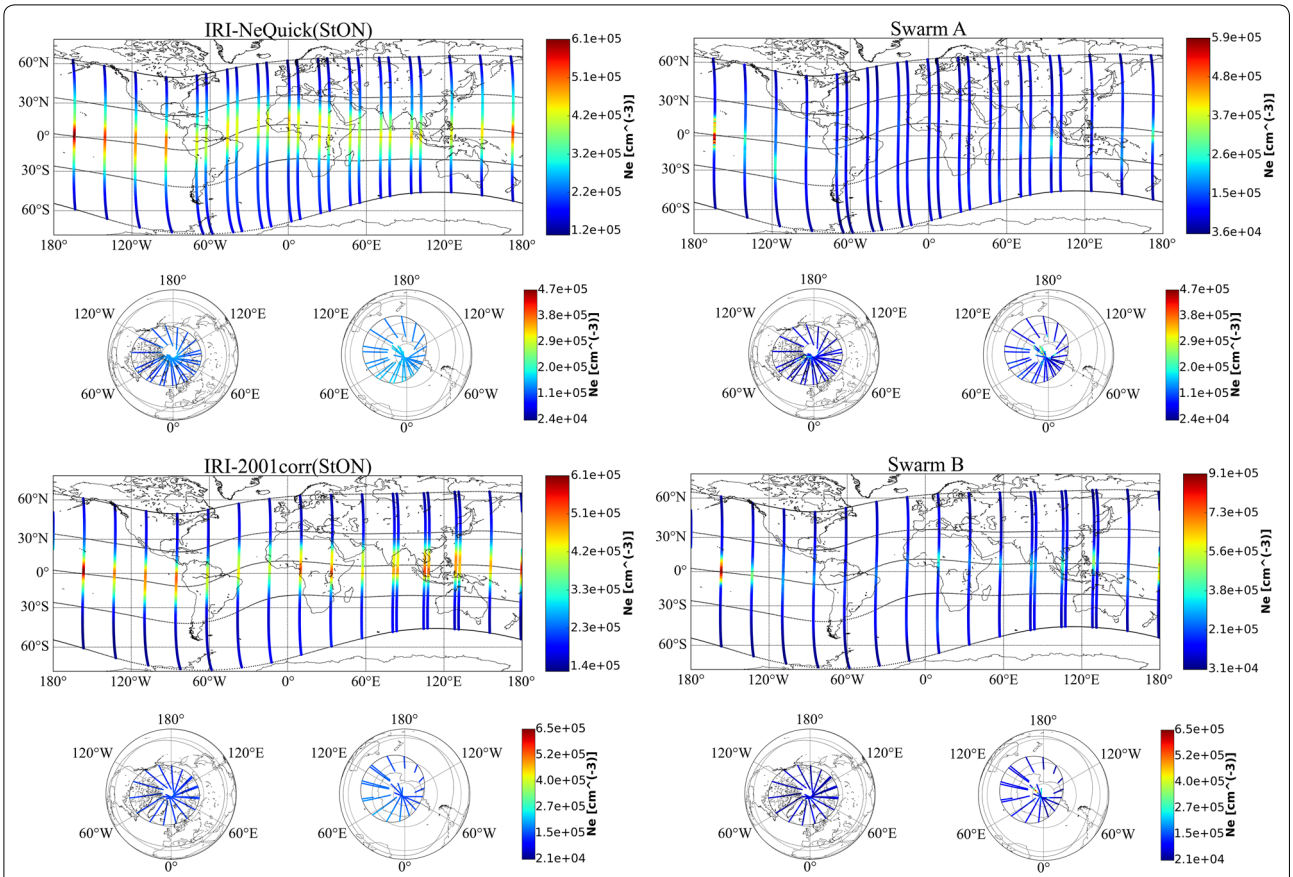

Fig. 8 Electron densities measured by Swarm satellites and IRI for period R1, for the morning sector. Same as Fig. 5, but for R1 morning sector

Concerning the polar regions, the values measured by Swarm satellites are pretty different from those given by IRI and, with regard to this, the most striking feature is the very low values of correlation coefficients characterizing the northern polar region for Swarm B (Fig. 14).

About periods M1/M2, for the morning sector (Figs. 6, 7), IRI still models an equatorial pattern characterized by a maximum centered on the magnetic equator, while Swarm measures a double-crest pattern in the west longitude sector of the globe, that is unusual for these local times. In fact, at these local times, the zonal electric field is westward and gives rise to a reverse fountain causing an increase of electron density around the magnetic equator, according to the mechanism proposed by Balan and Bailey (1995). The double-crest pattern measured by Swarm can be ascribed to an early fountain effect caused by ionospheric electric fields and currents that at low and mid-latitudes, during geomagnetic disturbed periods, can significantly differ from their quiet-day patterns, due to a concurrent action of two mechanisms: the magnetospheric dynamo and the ionospheric disturbance dynamo (Blanc and Richmond 1980). Dynamic interactions between the solar wind and the magnetosphere are the source of the magnetospheric dynamo. This gives rise to electrical currents which, along with their associated electric fields [called penetrating interplanetary electric fields (IEFs)], can penetrate to lower latitudes through the conducting ionosphere (Fejer and Scherliess 1995; Fejer et al. 2008; Huang et al. 2007; Zhao et al. 2008). The second mechanism is instead generated by an energy input to the thermosphere that alters the global thermospheric circulation, modifying the electric fields and currents that are generated by the ionospheric wind dynamo action during quiet conditions at low and mid-latitudes (Fejer et al. 2008; Nicolls et al. 2006).

Specifically, Fejer et al. (2008) showed that during equinox, for geomagnetically disturbed periods, the equatorial drifts ascribable to the magnetospheric dynamo are upward from about 07 to 23 LT, those due to the ionospheric dynamo are upward between 21 and 16 LT during equinox, with the amplitudes of daytime ones (between 07 and 16 LT) that are significantly lower than the nighttime ones (between 21 and 06 LT).

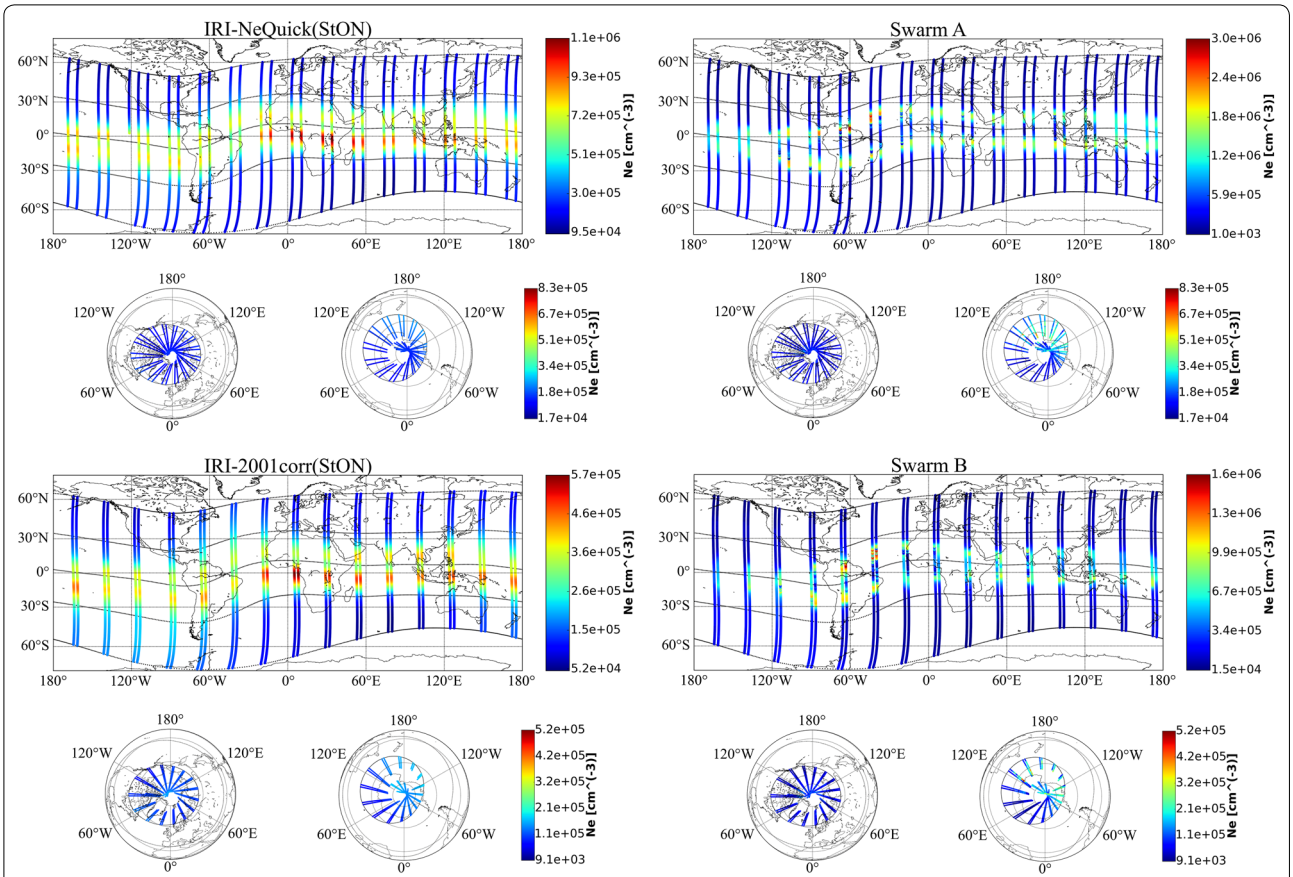

Fig. 9 Electron densities measured by Swarm satellites and IRI for period P1, for the evening sector. Same as Fig. 5, but for P1 evening sector

This further supports the thought that the double-crest pattern measured by Swarm in Figs. 6 and 7 is due to a combined effect of IEFs and the ionospheric disturbance wind dynamo, with a contribution of the latter which is definitely smaller, thus causing an inversion of the usual dynamo zonal electric field from westward to eastward. In particular, during the M1 period, two crests of electron density well beyond the magnetic parallels at 30° and −30° are observed in the Atlantic Ocean sector, suggesting also the occurrence of a "super-fountain effect" (Balan et al. 2010; Zong et al. 2010). It is interesting to note how the double-crest pattern in the M2 period is still recorded by Swarm A and not by Swarm B, suggesting that, in the 2 h of MLT difference characterizing the two satellites, the plasma fountain from direct became again reverse.

Also the polar patterns given by IRI are different from those measured by Swarm, showing a general overestimation of N_e. This feature is confirmed by the low values of correlation coefficients characterizing the polar bands (Figs. 13, 14), especially for Swarm B.

Regarding the period R1 (the same is for R2), for the morning sector (Fig. 8), Swarm comes back to the usual pattern characterized by a maximum centered on the magnetic equator, as on the other hand is modelled by IRI; anyway, along a Pacific Ocean sector, Swarm measures N_e values higher than IRI ones, while the rest of values are lower than those modelled by IRI. Again, the correlation coefficients of polar regions are the lowest ones, confirming that also for the R1 period Swarm and IRI patterns are different.

Concerning the period P1 (the same is for the period P2), for the evening sector (Fig. 9), the equatorial band shows for both IRI and Swarm the same usual electron density double-crest pattern around the magnetic equator (e.g., Balan and Bailey 1995). The values measured by Swarm that show a maximum over the south American sector are, however, higher than those given as output by IRI. Moreover, the IRI values are significantly asymmetric with those of the southern crest that are higher than those of the northern crest. On the contrary, Swarm

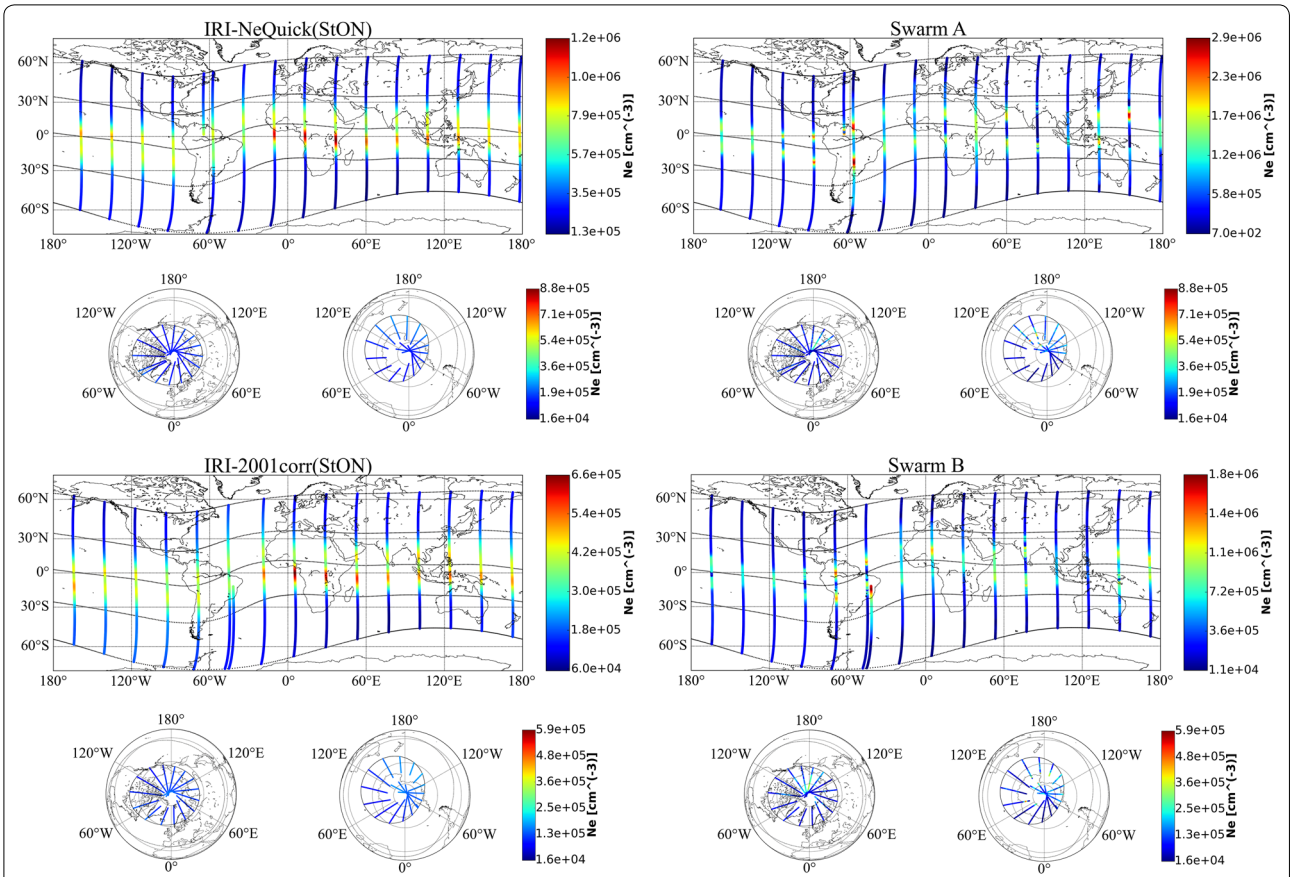

Fig. 10 Electron densities measured by Swarm satellites and IRI for period M1, for the evening sector. Same as Fig. 5, but for M1 evening sector

satellites measure two crests that are very similar, and there is only a slight difference over the South America, where Swarm presents the maximum of N_e, for which the northern crest is more intense than the southern one. As for the morning sector, also for the evening sector, the northern polar region is characterized by the lowest values of correlation coefficients (Figs. 13, 14).

With reference to periods M1/M2, for the evening sector (Figs. 10, 11), the usual electron density double-crest pattern around the magnetic equator is still shown by both IRI and Swarm, even though the crests measured by Swarm are noticeably narrower than those modelled by IRI. Anyway, also during the main phase of the storm, the values measured by Swarm, which present again a maximum over the South American sector, are higher than those modelled by IRI. Moreover, as for the period P1, IRI still models electron density crests that are significantly asymmetric, with the southern crest which is notably more intense than the northern one. It is not the same for the electron density crests measured by Swarm, which appear quite symmetric. During the main phase of the storm, the polar patterns characterizing IRI and Swarm are again sensibly different, especially for the period M2; the most striking feature is the very low values of correlation coefficient associated to the northern polar region.

Concerning the period R1 (the same is for the period R2), for the evening sector (Fig. 12), the morphology of all latitude bands is very similar to that of periods M1/M2. The only difference is that the maximum values of N_e measured by Swarm are now spread on a wider longitude sector including also the Atlantic Ocean.

In summary, Figs. 5, 6, 7, 8, 9, 10, 11, 12, 13, 14, and 15 show that, from a morphological point of view, the electron density patterns measured by Swarm and those modelled by IRI are different, especially during the main phase of the storm, for the morning sector, when Swarm highlights an unusual double-crest pattern. As a consequence, the correlation coefficients between IRI and Swarm of all magnetic latitude bands are somewhat low, mainly in the periods M1, M2, and R1. In general, the correlation coefficients of mid-latitude regions are higher than those of equatorial and polar regions, confirming a

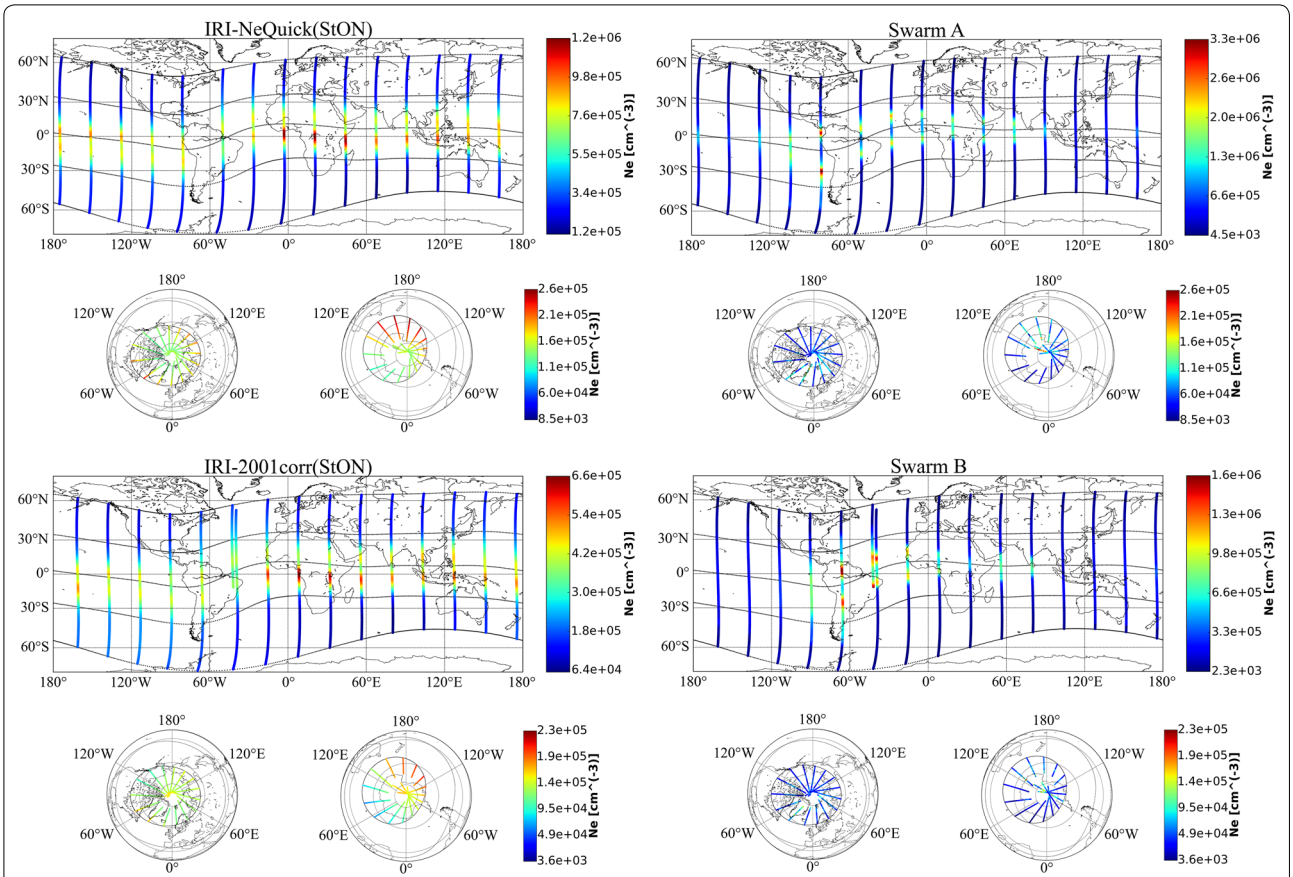

Fig. 11 Electron densities measured by Swarm satellites and IRI for period M2, for the evening sector. Same as Fig. 5, but for M2 evening sector

well-known feature of IRI, that is IRI predictions are less accurate at equatorial and auroral latitudes (Bilitza and Reinisch 2008).

The correlation coefficients of the northern polar region deserve a special mention, because they are often very low (even negative at times), for both the morning and evening sectors, and although less evident the same happens for the southern polar region. This result is most likely caused by the high-latitude current systems, which are activated during disturbed magnetic periods. In fact, the lowest values of correlation are found mainly in the periods M2 and R1. During these periods the a_p index, which is the magnetic index used by IRI, is not high ($a_p < 50$), especially when compared with that relative to the M1 period ($a_p > 150$). Nevertheless, the values of the *AE* index clearly show an intense global electrojet activity in the auroral zone during both the main and the recovery phases of the storm; this means that from 18 to 22 March 2015 the auroral regions are characterized by an intense substorm activity, with a consequent enhancement of the auroral electrojet systems. This may explain the considerable difference obtained between Swarm measurements and IRI modelled values not only at polar regions, but also between the morning and evening sectors. Indeed, the spatial distribution of the polar ionospheric convection and current systems is not uniform at high latitude, showing a greater intensity in the evening sector than in the morning one. Moreover, during this particular geomagnetic event, also a difference of the current intensities could have characterized the two hemispheres. This hypothesis is consistent with the results reported by Cherniak et al. (2015) who, during the St. Patrick geomagnetic storm, found hemispheric asymmetries in both the intensity and spatial structures of ionospheric irregularities.

An interesting feature showed by Swarm measurements during the analyzed periods is represented by the very low values of N_e, for the evening sector, as it is displayed in Fig. 16. The most striking feature of Fig. 16 is that for quiet periods these values are clustered along the magnetic equator, while during disturbed periods they are grouped at magnetic latitudes of about ±60°, with

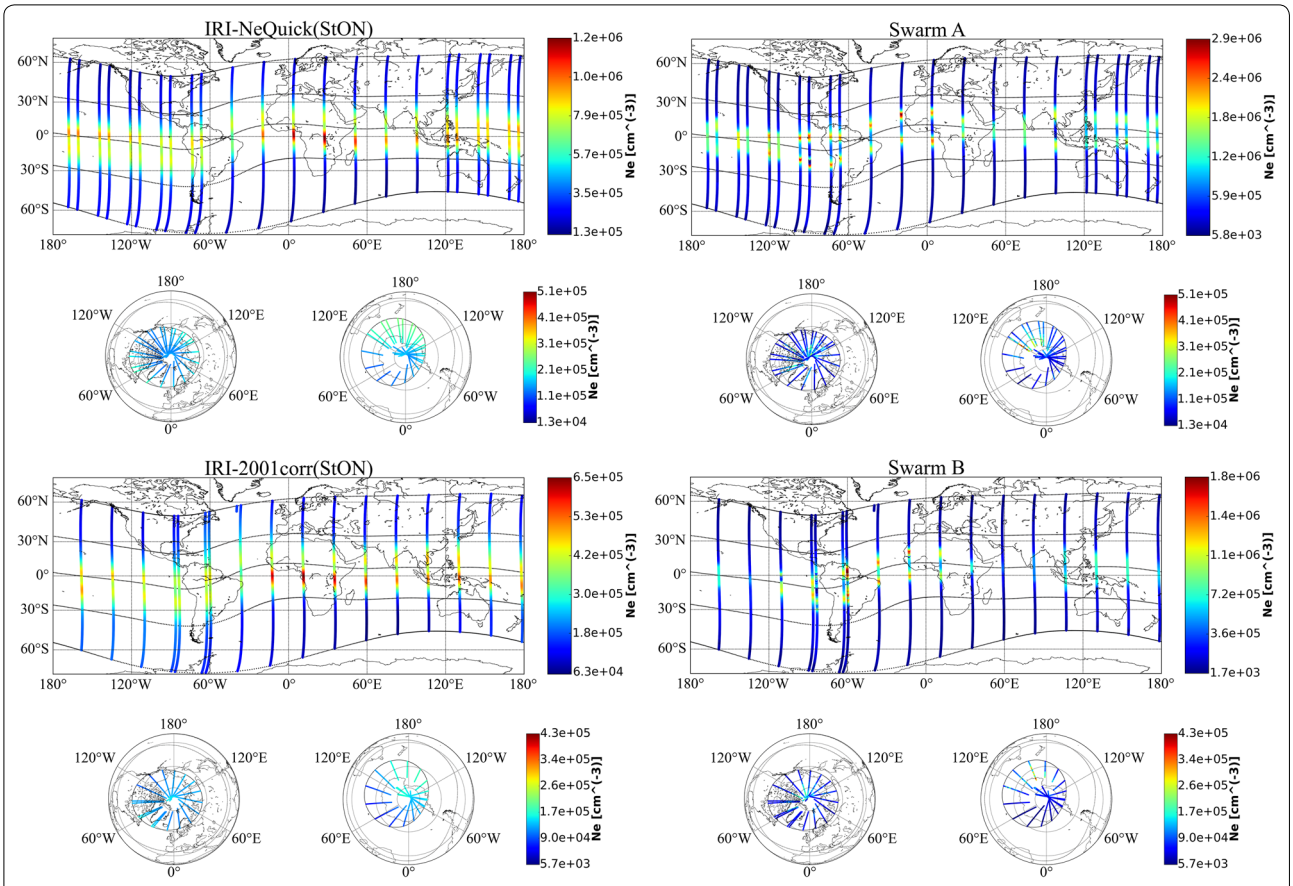

Fig. 12 Electron densities measured by Swarm satellites and IRI for period R1, for the evening sector. Same as Fig. 5, but for R1 evening sector

those of the recovery phase period being more rarefied than those of the main phase period.

The clusters along the magnetic equator can be interpreted as equatorial plasma bubbles. In fact, near sunset, plasma densities and dynamo electric fields in the E region decrease causing a weakening of the equatorial anomaly. At the same time, however, at this local time (corresponding to the evening sector here considered), a dynamo develops in the F region, and polarization charges within conductivity gradients at the terminator surface enhance the eastward electric field after sunset, giving rise to a pre-reversal increase of the equatorial fountain (Woodman 1970). Hence, in these hours, a rapid uplifting of the plasma in the F region and a general steepening of the bottom side gradient lead to the Rayleigh–Taylor instability, which allows plasma density irregularities to form. These irregularities can grow to become large ionospheric depletions that are usually called equatorial plasma bubbles (e.g., Whalen 2000). The fact that very low values of N_e are detected along the magnetic equator only during quiet conditions could be an additional confirmation that ionospheric irregularities can be either inhibited or triggered during disturbed periods, possibly depending on the phase of the storm and local time of occurrence of D_{st} maximum excursion (Aarons 1991; Alfonsi et al. 2013; Dabas et al. 2003).

Concerning the very low values of N_e measured by Swarm at magnetic latitudes of about $\pm 60°$, these are interpreted as the mid-latitude ionospheric trough, which is a latitudinal (located equatorward of the auroral oval) narrow and longitudinal extended depletion in the electron distribution, regularly detected in evening and night hours (Moffett and Quegan 1983). The ionospheric trough, characterized by very low values of N_e, is so well detected under disturbed conditions by Swarm satellites because, as shown by Krankowski et al. (2009), it significantly depends on the geomagnetic activity. In fact, under disturbed conditions, the ionospheric trough tends to exhibit much lower values of electron density than for quiet conditions. This is confirmed by what it is shown in Fig. 16. In some sense, this N_e decrease of the ionospheric trough simplifies significantly its detection

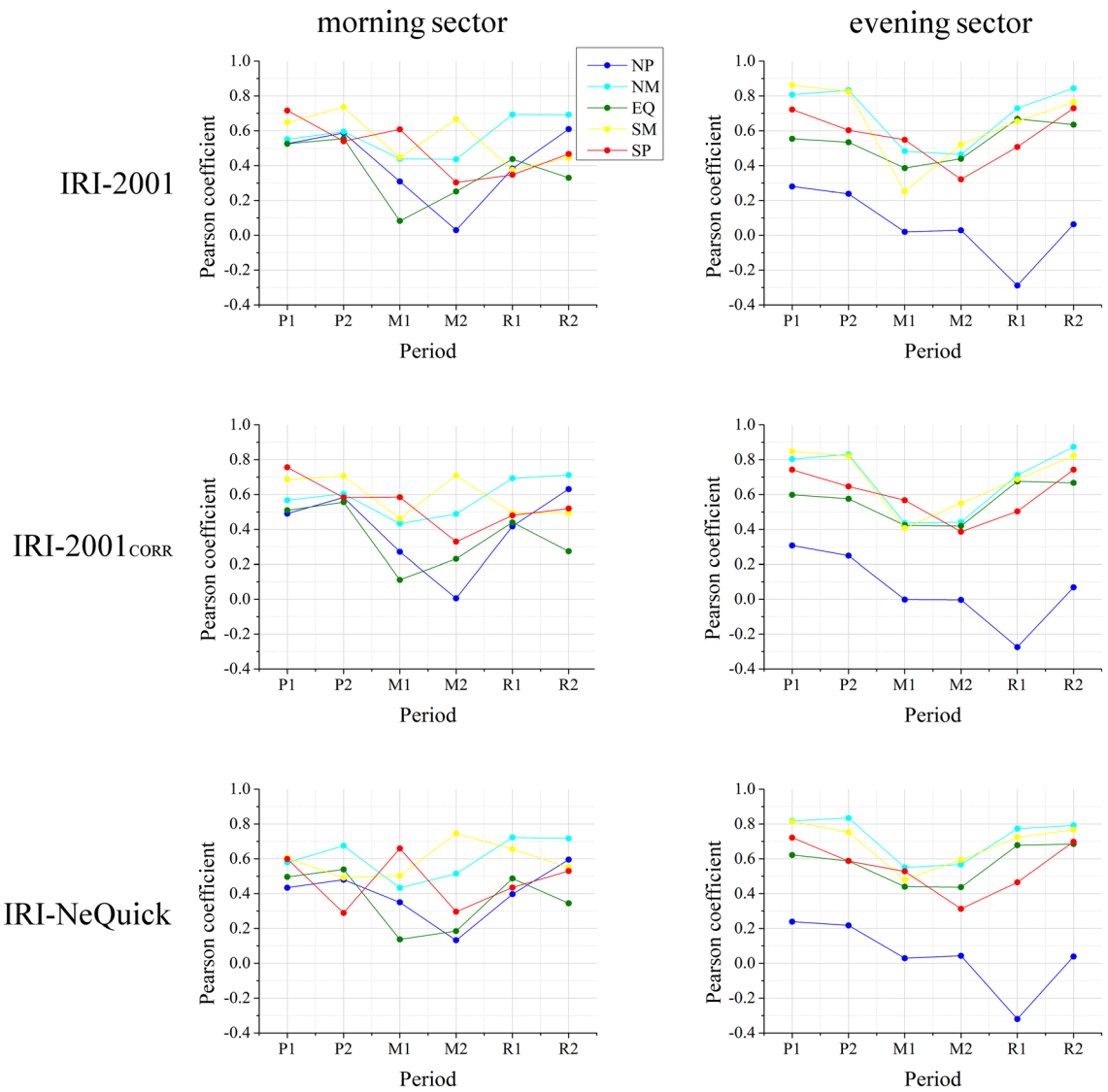

Fig. 13 Correlation analysis between Swarm A and C and IRI values. Average of Pearson coefficients calculated for Swarm A and C, for morning (*left panels*) and evening (*right panels*) sectors, for each magnetic latitude band (NP, NM, EQ, SM, SP), by considering all the three IRI topside models: IRI-2001 (*top panels*), IRI-2001corr (*middle panels*), and IRI-NeQuick (*bottom panels*)

in both hemispheres by Swarm satellites. As expected, this feature is not modelled by IRI, because at present the model has difficulties in reproducing auroral boundaries as well as density and temperature features related to these boundaries, such as the subauroral density trough (Bilitza et al. 2014).

Conclusions

This work represents a further evidence that the topside ionosphere modelling, especially during magnetically disturbed periods, is still a challenge. In fact, even though they are preliminary, Swarm electron density data considered in this study, measured during March 2015 including the St. Patrick storm, showed patterns that are at the moment difficult to model. Specifically, the analysis we have done, based on the Pearson correlation coefficient, showed that, independently of the chosen topside option (IRI-2001, IRI-2001corr, NeQuick), the trends embedded in the Swarm and IRI time series are fairly different. In particular, the analysis did not show a topside option that behaves definitely better than the others.

For the sake of correctness, it is worth reminding that the IRI model works the best when considering long

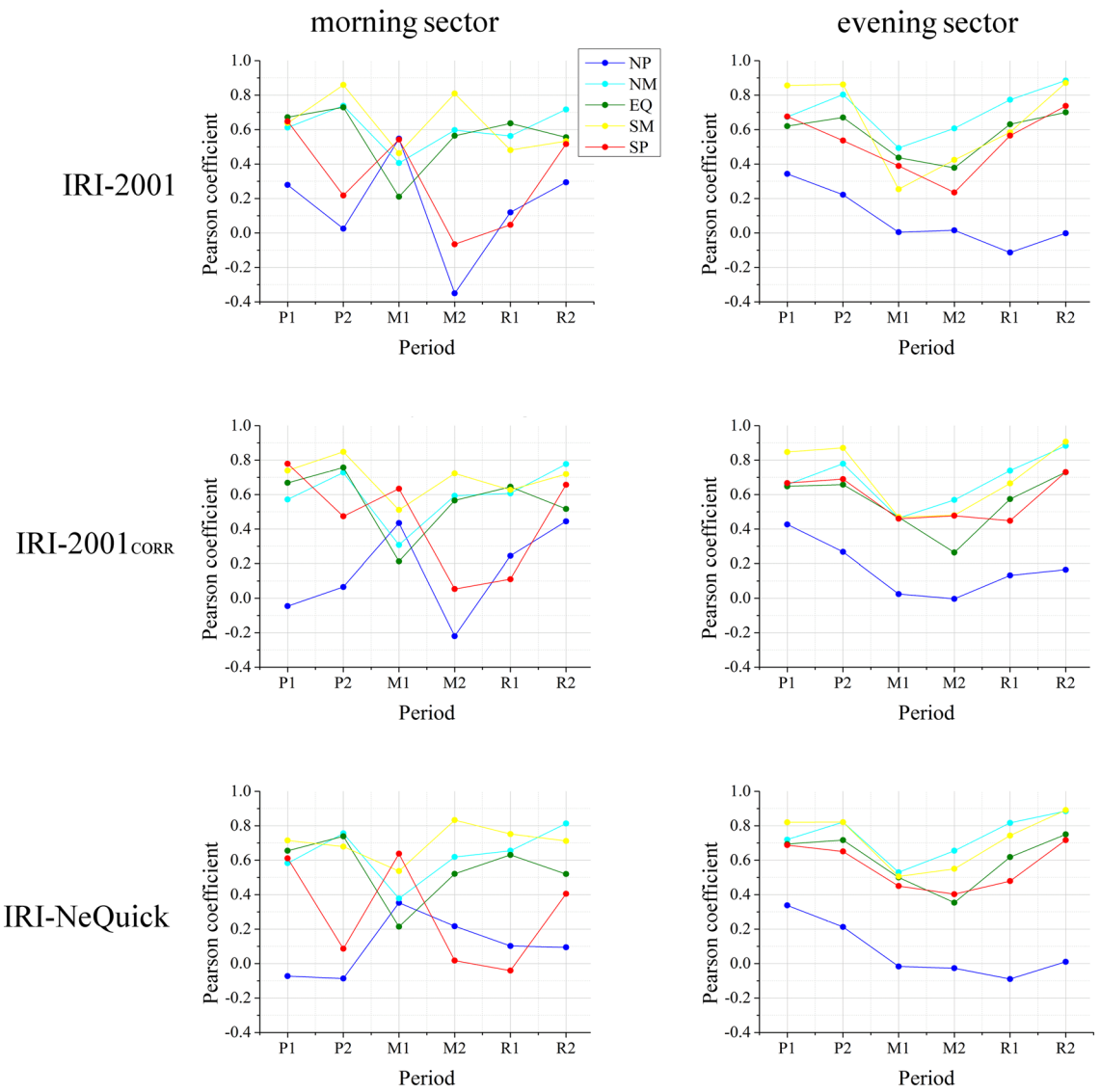

Fig. 14 Correlation analysis between Swarm B and IRI values. Pearson coefficients calculated for Swarm B, for morning (*left panels*) and evening (*right panels*) sectors, for each magnetic latitude band (NP, NM, EQ, SM, SP), by considering all the three IRI topside models: IRI-2001 (*top panels*), IRI-2001corr (*middle panels*), and IRI-NeQuick (*bottom panels*)

series of monthly median values, while in this work the IRI model was compared directly with plasma measurements on a limited period of time. So, to fully confirm the results here described, longer series of monthly median values should be considered. At the same time, however, we would like to stress the fact that if this might be possible for quiet periods, it would become difficult when considering disturbed conditions, for which the calculation of monthly median values does not make sense. On the other hand, given that the IRI model has a "*storm*" routine capable of changing the output of the model for disturbed conditions, the results here shown, although based on a limited series of data, have their own validity.

With regard to the topside modelling, in situ measurements of the thin electron plasma density around the Earth carried out by the Swarm constellation can be extremely valuable. In fact, when having accurate and calibrated measurements, the peculiar configuration of Swarm satellites will allow to achieve new insights about

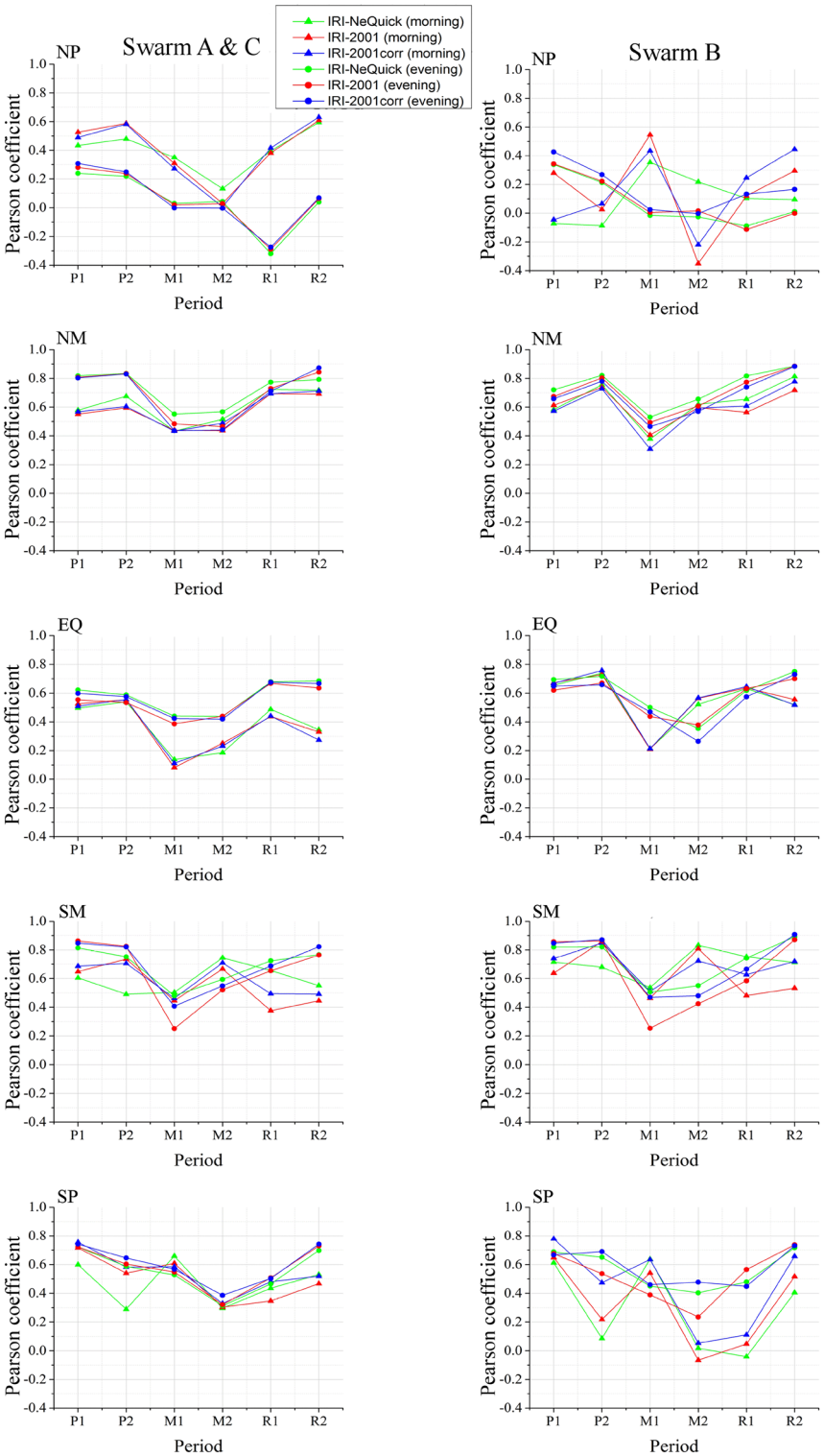

Fig. 15 Magnetic latitude dependence of Pearson coefficients calculated between Swarm satellites and IRI values. Average of Pearson coefficients calculated for Swarm A and C (*left panels*), and Pearson coefficients calculated for Swarm B (*right panels*), for each magnetic latitude band (from *top* to *bottom*: NP, NM, EQ, SM, and SP), by considering all the three IRI topside models (IRI-2001, IRI-2001corr, IRI-NeQuick), for morning and evening sectors

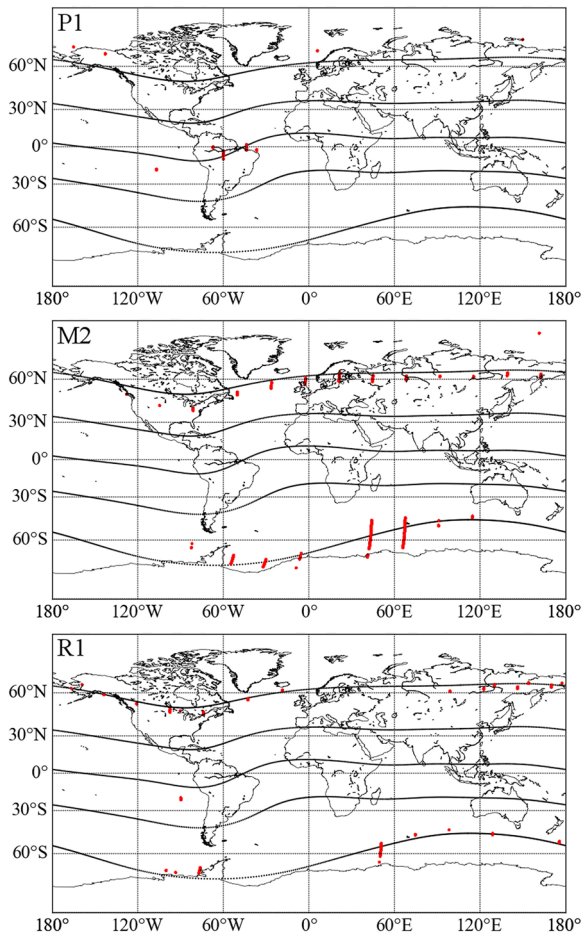

Fig. 16 Very low values of electron density measured by Swarm A for the evening sector. Swarm A electron density values (in *red*) lower than 2×10^4 cm^{-3}, for periods P1 (*top panel*), M2 (*middle panel*), and R1 (*bottom panel*), for the evening sector. Coordinates are geographical, and *bold lines* represent magnetic parallels drawn with a 30° step

the topside plasma scale height, a parameter of crucial significance to reliably model the topside profile.

Abbreviations

EFI: Electric field instrument; EQ: equator; ESA: European Space Agency; IEF: interplanetary electric field; IMF: interplanetary magnetic field; IRF: Swedish Institute for Space Science; IRI: International Reference Ionosphere; ISO: International Standardization Organization; LP: Langmuir probe; MLT: magnetic local time; NM: north mid; NP: north pole; SM: south mid; SP: south pole; TII: thermal ion imager; URSI: International Union of Radio Science; UT: Universal Time.

Authors' contributions

AP made all the analyses needed to compare Swarm and IRI trends. MP conceived and coordinated the study and discussed the results. RT participated in designing the study, prepared the Swarm dataset, and helped to draft the manuscript. PDM participated in the discussion concerning the influence of geomagnetic storms and substorms on the geospace and helped to draft the manuscript. IC actively participated in the discussion concerning the reliability of Swarm Langmuir probe measurements. All authors read and approved the final manuscript.

Author details

[1] Dipartimento di Fisica e Astronomia, Università di Bologna "Alma Mater Studiorum", Viale Carlo Berti Pichat 6/2, 40127 Bologna, Italy. [2] Istituto Nazionale di Geofisica e Vulcanologia, Via di Vigna Murata 605, 00143 Rome, Italy. [3] Serco Italia S.P.A., Via Sciadonna 24/26, 00044 Frascati, RM, Italy.

Acknowledgements

We thank all members of the ESA Swarm team for their precious work, which is the basis for our investigations; in particular, we thank Dr. Stephan Buchert of Swedish Institute of Space Physics (IRF) for having made available the Langmuir Probes Preliminary Plasma Dataset, freely accessible at https://earth.esa.int/web/guest/swarm/data-access. We acknowledge use of NASA/GSFC's Space Physics Data Facility's CDAWeb service, and OMNI data that were obtained at http://cdaweb.gsfc.nasa.gov/. We acknowledge the IRI Working Group for their valuable work and for making the IRI code freely available at http://irimodel.org/.

Competing interests

The authors declare that they have no competing interests.

Received: 30 December 2015 Accepted: 6 May 2016
Published online: 28 May 2016

References

Aarons J (1991) The role of the ring current in the generation or inhibition of equatorial F layer irregularities during magnetic storms. Radio Sci 26:1131–1149. doi:10.1029/91RS00452

Alfonsi L, Spogli L, Pezzopane M, Romano V, Zuccheretti E, De Franceschi G, Cabrera MA, Ezquer RG (2013) Comparative analysis of spread-F signature and GPS scintillation occurrences at Tucuman, Argentina. J Geophys Res Space Phys 118:4483–4502. doi:10.1002/jgra.50378

Araujo-Pradere EA, Fuller-Rowell TJ, Codrescu MV (2002) STORM: an empirical storm-time ionospheric correction model 1. Model description. Radio Sci. doi:10.1029/2001RS002467

Balan N, Bailey GJ (1995) Equatorial plasma fountain and its effect: possibility of an additional layer. J Geophys Res 100:21421–21432

Balan N, Shiokawa K, Otsuka Y, Kikuchi T, Vijaya Lekshmi D, Kawamura S, Yamamoto M, Bailey GJ (2010) A physical mechanism of positive ionospheric storms at low latitudes and midlatitudes. J Geophys Res 115:A02304. doi:10.1029/2009JA014515

Benson RF, Reinisch BW, Green JL, Fung SF, Calvert W, Haines DM, Bougeret JL, Manning R, Carpenter DL, Gallagher DL, Reiff P, Taylor WWL (1998) Magnetospheric radio sounding on the IMAGE mission. Radio Sci Bull 285:9–20

Bilitza D (2001) International Reference Ionosphere 2000. Radio Sci 36:261–275. doi:10.1029/2000RS002432

Bilitza D (2004) A correction for the IRI topside electron density model based on Alouette/ISIS topside sounder data. Adv Space Res 33:838–843

Bilitza D, Reinisch BW (2008) International Reference Ionosphere 2007: improvements and new parameters. Adv Space Res 42:599–609. doi:10.1016/j.asr.2007.07.048

Bilitza D, Reinisch BW (2015) Preface: International Reference Ionosphere and global navigation satellite systems. Adv Space Res 55:1913

Bilitza D, Reinisch BW, Radicella SM, Pulinets S, Gulyaeva T, Triskova L (2006) Improvements of the International Reference Ionosphere model for the topside electron density profile. Radio Sci. 41:RS5S15. doi:10.1029/2005RS003370

Bilitza D, Altadill D, Zhang Y, Mertens C, Truhlik V, Richards P, McKinnell LA, Reinisch B (2014) The International Reference Ionosphere 2012—a model of international collaboration. J Space Weather Space Clim 4:A07. doi:10.1051/swsc/2014004

Blanc M, Richmond AD (1980) The ionospheric dynamo. J Geophys Res 85:1669–1686

Cherniak I, Zakharenkova I, Redmon RJ (2015) Dynamics of the high-latitude ionospheric irregularities during the 17 March 2015 St. Patrick's Day

storm: ground-based GPS measurements. Space Weather. doi:10.1002/2015SW001237
Coisson P, Radicella SM, Leitinger R, Ciraolo L (2004) Are models predicting a realistic picture of vertical total electron content? Radio Sci 39:RS1S14. doi:10.1029/2002RS002823
Coisson P, Radicella SM, Leitinger R, Nava B (2006) Topside electron density in IRI and NeQuick: features and limitations. Adv Space Res 37:934–937
Dabas RS, Singh L, Lakshmi DR, Subramanyam P, Chopra P, Garg SC (2003) Evolution and dynamics of equatorial plasma bubbles: relationships to E × B drift, postsunset total electron content enhancements and equatorial electrojet strength. Radio Sci 38(4):1075. doi:10.1029/2001RS002586
Davies K (1990) Ionospheric Radio. Peter Peregrinus Ltd., London
Emmert JT, Richmond AD, Drob DP (2010) A computationally compact representation of Magnetic-Apex and Quasi-Dipole coordinates with smooth base vectors. J Geophys Res. doi:10.1029/2010JA015326
Fejer BG, Scherliess L (1995) Time dependent response of equatorial ionospheric electric field to magnetospheric disturbances. Geophys Res Lett 22:851–854
Fejer BG, Jensen JW, Su S-Y (2008) Seasonal and longitudinal dependence of equatorial disturbance vertical plasma drifts. Geophys Res Lett 35:L20106. doi:10.1029/2008GL035584
Friis-Christensen E, Lühr H, Hulot G (2006) *Swarm*: a constellation to study the Earth's magnetic field. Earth Planets Space 58:351–358
Fuller-Rowell TJ, Araujo-Pradere E, Codrescu MV (2000) An empirical ionospheric storm-time correction model. Adv Space Res 25(1):139–146
Huang XQ, Reinisch BW (2001) Vertical electron content from ionograms in real time. Radio Sci 36:335–342
Huang X, Reinisch BW, Bilitza D, Benson RF (2002) Electron density profiles of the topside ionosphere. Ann Geophys Italy 45:125–130
Huang C-S, Sazykin S, Chau JL, Maruyama N, Kelley MC (2007) Penetration electric fields: efficiency and characteristic time scale. J Atmos Sol Terr Phys 69:1135–1146. doi:10.1016/j.jastp.2006.08.016
Immel TJ, Sagawa E, England SL, Henderson SB, Hagan ME, Mende SB, Frey HU, Swenson CM, Paxton LJ (2006) Control of equatorial ionospheric morphology by atmospheric tides. Geophys Res Lett 33:L15108. doi:10.1029/2006GL026161
Jee G, Schunk RW, Scherliess L (2005) Comparison of IRI-2001 with TOPEX TEC measurements. J Atmos Solar-Terr Phys 67:365–380. doi:10.1016/j.jastp.2004.08.005
Kamide Y, Kusano K (2015) No major solar flares but the largest geomagnetic storm in the present solar cycle. Space Weather 13:365–367. doi:10.1002/2015SW001213
Kelley MC (2009) The Earth's ionosphere. International Geophysics (Book 96), 2nd edn. Academic Press, San Diego
Knudsen D, Burchill J, Buchert S, Coco I, Toffner-Clausen L, Holmdahl Olsen PE (2015) Swarm preliminary Plasma dataset User Note, ESA Ref. SWAM-GSEG-EOPG-TN-15-0003. https://earth.esa.int/web/guest/document-library/browse-document-library/-/article/swarm-preliminary-plasma-dataset-user-note
Krankowski A, Shagimuratov II, Ephishov II, Krypiak-Gregorczyk A, Yakimova G (2009) The occurrence of the mid-latitude ionospheric trough in GPS-TEC measurements. Adv Space Res 43:1721–1731. doi:10.1016/j.asr.2008.05.014
Liu H, Thampi SV, Yamamoto M (2010) Phase reversal of the diurnal cycle in the midlatitude ionosphere. J Geophys Res 115:A01305. doi:10.1029/2009JA014689
Lühr H, Rother M, Häusler K, Fejer B, Alken P (2012) Direct comparison of non-migrating tidal signatures in the electrojet, vertical plasma drift and equatorial ionization anomaly. J Atmos Solar-Terr Phys 75–76:31–43. doi:10.1016/j.jastp.2011.07.009
Moffett RJ, Quegan S (1983) The mid-latitude trough in the electron concentration of the ionospheric F-layer: a review of observations and modeling. J Atmos Terrest Phys 45:315–343
Nicolls MJ, Kelley MC, Vlasov MN, Sahai Y, Chau JL, Hysell DL, Fagundes PR, Becker-Guedes F, Lima WLC (2006) Observations and modeling of post-midnight uplifts near the magnetic equator. Ann Geophys 24:1317–1331. doi:10.5194/angeo-24-1317-2006
Pedatella N, Stolle C, Chau J (2015) Comparing Swarm electron density data to COSMIC GPS radio occultation observations. Paper presented at the 26th IUGG General Assembly, Prague, Czech Republic, June 22–July 2 2015
Radicella SM, Leitinger R (2001) The evolution of the DGR approach to model electron density profiles. Adv Space Res 27:35–40
Radicella SM, Zhang M-L (1995) The improved DGR analytical model of electron density height profile and total electron content in the ionosphere. Ann Geophys 38(1):35–41
Reinisch BW, Huang XQ (2001) Deducing topside profiles and total electron content from bottomside ionograms. Adv Space Res 27:23–30
Sagawa E, Immel TJ, Frey HU, Mende SB (2005) Longitudinal structure of the equatorial anomaly in the nighttime ionosphere observed by IMAGE/FUV. J Geophys Res 110:A11302. doi:10.1029/2004JA010848
Whalen JA (2000) An equatorial bubble: its evolution observed in relation to bottomside spread F and to the Appleton anomaly. J Geophys Res 105:5303–5315
Woodman RF (1970) Vertical drift velocities and east-west electric fields at the magnetic equator. J Geophys Res 75(31):6249–6259. doi:10.1029/JA075i031p06249
Xiong C, Luhr H (2014) The Midlatitude Summer Night Anomaly as observed by CHAMP and GRACE: interpreted as tidal features. J Geophys Res Space Phys 119:4905–4915. doi:10.1002/2014JA019959
Zhao B, Wan W, Liu L, Igarashi K, Nakamura M, Paxton LJ, Su SY, Li G, Ren Z (2008) Anomalous enhancement of ionospheric electron content in the Asian-Australian region during a geomagnetically quiet day. J Geophys Res 113:A11302. doi:10.1029/2007JA012987
Zong Q-G, Reinisch BW, Song P, Wei Y, Galkin IA (2010) Dayside ionospheric response to the intense interplanetary shocks–solar wind discontinuities: observations from the digisonde global ionospheric radio observatory. J Geophys Res 115:A06304. doi:10.1029/2009JA014796